



CHORUS

This is the accepted manuscript made available via CHORUS. The article has been published as:

Influence of spatial inhomogeneity on electronic and magnetotransport in graphene

Bernard R. Matis, Brian H. Houston, and Jeffrey W. Baldwin

Phys. Rev. B **91**, 205406 — Published 11 May 2015

DOI: [10.1103/PhysRevB.91.205406](https://doi.org/10.1103/PhysRevB.91.205406)

The Influence of Spatial Inhomogeneity on the Electronic and Magneto Transport in Graphene

Bernard R. Matis^{1,*}, Brian H. Houston¹, and Jeffrey W. Baldwin¹

¹ Naval Research Laboratory, Code 7130, Washington, DC 20375, United States

*Correspondence to: bernard.matis@nrl.navy.mil

Abstract:

We present room temperature electronic and magnetotransport measurements of polycrystalline graphene, grown by chemical vapor deposition, on a SiO₂ dielectric. The measured graphene devices are intentionally spatially inhomogeneous such that the length of the sample is much greater (>1000 times) than the average grain size. At magnetic field $B = 0$ T the electronic transport is well described by a diffusive transport model with contributions from grain boundary scattering significantly larger in the high charge carrier density limit. We find the largest percent change in the magnetoresistivity occurs at the film's Dirac point where the magnetotransport is largely dependent upon charge disorder. Away from the Dirac point we find a modified expression for the charge carrier density dependence of the magnetoresistivity with respect to the case of single-crystal graphene.

I. Introduction

The ability to grow large-scale, high-quality graphene films is critical for the development of commercial graphene-based applications, such as magnetoelectric sensors and data storage systems. Chemical vapor deposition (CVD) is one growth method that holds promise for achieving such large-scale graphene production.¹⁻⁴ Graphene grown by CVD is polycrystalline, thus it is comprised of various grain boundaries that are formed at the point where neighboring grains merge together during the growth process. Gaining an understanding of how these grains affect graphene's electronic and magnetotransport is essential for the development of graphene-based technologies.

Grain boundaries produced during the CVD growth method can negatively impact overall device quality. Thus far, studies have primarily focused on the single grain boundary limit, providing direct evidence of how such a defect in the crystal lattice can affect the graphene transport.⁵⁻⁸ These studies have shown, for example, that the presence of a grain boundary within the graphene film can lead to an increase in charge carrier scattering resulting in a reduction in both the electrical conductivity σ and charge carrier mobility μ . While much effort has addressed the effect of individual grain boundaries on graphene's electronic properties, little attention has been paid to the scenario in which the transport occurs across many grain boundaries when the characteristic device size is much greater than the individual grain size. It is important to understand the role of the collection of grain boundaries as this introduces inhomogeneous disorder that can lead to, for example, effects such as Anderson localization and

enhanced short-range scattering, which can have implications on the electronic and magnetotransport properties of the material.

Thus far experimental studies of the magnetotransport in CVD-derived graphene have focused on understanding quantum effects occurring at temperatures $T \leq 100$ K. For example, observations of the T dependence of Shubnikov-de Hass oscillations indicate that scattering lengths in polycrystalline graphene are comparable to that of exfoliated graphene, which suggests to some extent a preservation of graphene's intrinsic properties in disordered, polycrystalline graphene.⁹ Other measurements have revealed localization effects in CVD-derived graphene showing, for example, that individual graphene boundaries can induce weak localization.^{6,7,9,10} However, a complete study of the magnetotransport for $T > 100$ K and across a wide range of charge carrier density n is still lacking. Such experiments are important for understanding the overall influence of grain boundaries on the magnetotransport.

Here, we study electronic and magnetotransport in polycrystalline, CVD-grown graphene at $T = 293$ K and for a wide range of n . Our devices consist of many grains such that $L \gg L_a$, where L and L_a are the device length and average grain size, respectively. The measured electronic transport at magnetic field $B = 0$ T is well described by a diffusive transport model that takes into account uncorrelated charged impurity scattering, short-range scattering, and acoustic phonon scattering. These measurements shed light on the contribution from grain boundary scattering to the overall measured resistivity, with the largest contribution occurring in the limit of high n . Magnetotransport measurements reveal that the magnetoresistivity is dominated by charge disorder at low n and allow us to acquire a modified expression for the charge carrier density dependence of the magnetoresistivity with respect to the case of single-crystal graphene.

II. Experimental Methods

Our devices consist of polycrystalline graphene grown by CVD on Cu foil that has been transferred to a SiO₂ (285 nm)/Si (doped) substrate. An optical image of one of our devices can be seen in Fig. 1(a). An oxygen plasma is used to etch the graphene into a Hall bar geometry, and electron-beam lithography is used to define the Cr (10 nm)/Au (50 nm) contact electrodes. All of our electrical and magnetotransport measurements were carried out in vacuum ($< 3.0 \times 10^{-7}$ Torr) using a 4-contact configuration with a source current $I = 31.6$ nA and AC lock-in techniques at a frequency $f = 13.7$ Hz. In total, eight devices were tested in this study, all of which displayed the same qualitative behavior. All of the data sets presented were captured at $T = 293$ K.

Figure 1(b) shows an example of a Raman spectrum collected for one of our devices and taken under ambient conditions. For this particular device we measured $I_{2D}/I_G \sim 1.8$ and $I_D/I_G \sim 0.04$ indicating a single-layer film, where I_{2D} , I_D , and I_G are the 2D, D, and G band intensities, respectively. A rough estimate of L_a is found from $L_a^2(\text{nm}^2) = (1.8 \times 10^{-9})\lambda^4(I_G/I_D)$, where $\lambda = 514$ nm is the excitation wavelength.¹¹ From the data shown in Fig. 1(b) we find $L_a \sim 37.7$ nm, which is 3 orders of magnitude smaller than the region of the Hall bar measured using a 4-contact configuration (between contacts 3 and 4 in Fig. 1(a)). For the eight devices tested we found $27.1 \text{ nm} \leq L_a \leq 41.5 \text{ nm}$ with an average $L_a \sim 34.6$ nm. These L_a values suggest that our graphene Hall bars are spatially inhomogeneous and contain many grain boundaries throughout the film.

III. Results

Figure 1(c) shows σ versus n at $B = 0$ T for one of our devices. Values for σ were obtained from $\sigma = L/RW$ where L and W are the sample length and width, respectively, and R is the sample resistance obtained by sourcing a current between electrodes 1 and 2, I_{12} , as labeled in Fig. 1(a) and by measuring the resultant voltage drop along the current path using electrodes 3 and 4, V_{34} . Applying a back gate voltage V_g to the doped Si substrate allows us to vary n . We determine n from $n = 1/eR_H$ where e is the fundamental unit of electric charge and R_H is the Hall coefficient, defined as $R_H = R_{xy}/B$. R_{xy} was found from $R_{xy} = V_{78}/I_{12}$ (Fig. 1(a)) with $B = 2.6$ T applied perpendicular to the plane of the graphene (further Hall effect information can be found in Ref. 12). The data plotted in Fig. 1(c) is shown in order to highlight the clear sublinear dependence of σ on n . The sublinear dependence of σ on n has been reported in the literature for exfoliated and single-crystal CVD-derived graphene and is a result of the various scattering mechanisms occurring within the film.¹³⁻¹⁶

The data in Fig. 1(c) is well fitted by a diffusive transport model given by

$$\sigma(n) = \left(\frac{1}{ne\mu_L} + \rho_s + \rho_{ph} \right)^{-1} \quad (1)$$

where μ_L is the n -independent mobility due to long-range, uncorrelated charged impurity scattering, and ρ_s and ρ_{ph} are the contributions to the resistivity due to short-range scattering and acoustic phonon scattering, respectively. Here, μ_L and ρ_s are the free fitting parameters and $\rho_{ph} = (0.1 \text{ } \Omega/\text{K}) \times T$.¹⁷ From the fits to the data we find $\mu_L \sim 0.5 \text{ m}^2/\text{Vs}$ for both electrons and holes while $\rho_s \sim 322 \Omega$ (204Ω) for electrons (holes). The values obtained for ρ_s are nearly an order of magnitude larger than those obtained for exfoliated graphene on SiO_2 ,¹³ which we attribute to the

polycrystalline nature of the graphene. The values obtained for μ_L are comparable to the measured values for the Hall mobility μ_H , however, μ_H was found to have a small dependence on n .¹²

Short-range scattering is expected to be the dominant scattering mechanism at the graphene grain boundary.^{5-7,18} If we are to assume that grain boundaries account for the entire ρ_s value (neglecting other scattering mechanisms such as point defects) then this demands that scattering from grain boundaries accounts for $\sim 50\%$ of the overall measured resistivity at the highest n ($\rho_s/\rho_e \sim 322 \text{ } \Omega / 587 \text{ } \Omega = 0.55$ and $\rho_s/\rho_h \sim 204 \text{ } \Omega / 471 \text{ } \Omega = 0.43$, where ρ_e and ρ_h are the measured resistivity at the highest electron and hole concentrations, respectively) while at the Dirac point (DP) scattering from grain boundaries accounts for less than 10% of the overall measured resistivity ($\rho_s/\rho_{DP} \sim 322 \text{ } \Omega / 4,489 \text{ } \Omega = 0.07$). This result suggests that at $T = 293 \text{ K}$ scattering from grain boundaries contributes only a fraction to the overall measured resistivity while charged impurity scattering is also significant. Therefore, even in such polycrystalline graphene films, where $L_a \ll L$, short-range scattering due to grain boundaries is not a dominant scattering mechanism at zero magnetic flux density and charged impurity scattering still contributes significantly to the overall resistivity.

A second method of quantifying the disorder present in our samples is through the full width at half maximum ΔW_{DP} of the $\rho = 1/\sigma$ vs. n peak. This results in an upper bound for the carrier density fluctuations δn_{max} due to charge carrier puddle formation at low n . For the data shown in Fig. 1(c) we find $\delta n_{max} \sim 5.5 \times 10^{15} \text{ m}^{-2}$. This value for δn_{max} is comparable to that observed for exfoliated graphene on SiO_2 .¹⁹⁻²¹ Scanning tunneling microscopy studies have also shown that grain boundaries tend to be more n -type relative to the bulk of the graphene and can

form local p-n-p or p-p'-p ($p' < p$) potential barriers.⁵ However, that the value for δn_{max} found here for polycrystalline graphene on SiO₂ is comparable to that of exfoliated graphene on SiO₂ suggests that on a global scale the local potential barriers established between neighboring grains do not significantly contribute, either positively or negatively, to the charge carrier puddle formation near the DP. Furthermore, for the data shown in Fig. 1(c) we find $V_{DP} \sim 0$ V, which suggests little intrinsic doping within our graphene film. Therefore, we suspect that charge carrier puddle formation and the contribution from charged impurity scattering are most likely due to the underlying SiO₂ substrate without significant contributions from grain boundaries.

Figure 2 shows the measured longitudinal resistivity $\rho_{xx} = R_{xx}W/L$ as a function of V_g for several values of B (B is always applied perpendicular to the graphene plane). Here, the largest change in the resistivity $\Delta\rho_{xx} = [\rho_{xx}(B) - \rho_{xx}(0)]$ occurs at the DP and we find that $\Delta\rho_{xx}$ decreases with increasing concentrations of electrons n_e ($V_g > 0$) and holes n_h ($V_g < 0$). We find similar magnetoresistive behavior for both n_e and n_h (see the sample traces in the Ref. 12). The magnetoresistive sensitivity of the graphene to a variation in n is highest near the film's DP. Near the DP any small change in n will result in a substantial change in $\Delta\rho_{xx}$. For our experiments we used $\Delta V_g = 2$ V, however, smaller step sizes in ΔV_g could result in larger values of $\Delta\rho_{xx}$ being obtained as n approaches the theoretical minimum and the Fermi energy E_F is shifted even closer to the DP. Additionally, the value of R_{xx} did not depend upon choice of measurement configuration: for example, at a fixed field strength of $B=2.6$ T measurements of the R_{xx} versus V_g using as voltage probes contacts 3 and 4, V_{34} , and using contacts 5 and 6, V_{56} , (see Fig. 1(a)) yielded equivalent results (See Fig. S5 in Ref 12). Therefore, we can exclude any direct geometry-induced contributions (or contributions from the Hall voltage, V_{xy}) to the measured R_{xx} values.

Figure 3 shows the percent change in the longitudinal resistivity $\Delta\rho_{xx}/\rho_0 = \{[\rho_{xx}(B) - \rho_{xx}(B=0 \text{ T})]/\rho_{xx}(B=0 \text{ T})\} \times 100$, as a function of B at the DP. Here, the data was captured using a field step size $\Delta B = 0.2 \text{ T}$. The data plotted in Fig. 3 shows that $\Delta\rho_{xx}/\rho_0$ is symmetric for both positive and negative B , which again indicates no direct Hall contribution to the measured R_{xx} values. The zero field resistivity ρ_0 is $\sim 4,900 \text{ } \Omega$ and increases to roughly 106 % of its initial value at $B = \pm 2.6 \text{ T}$. Also plotted in Fig. 3 is a fit to the data according to a theory for a macroscopically disordered 2-dimensional (2D) conductor that takes into account an inhomogeneous distribution of electrons and holes throughout the conductor with equal mobility and equal concentrations,²² which is given by

$$\rho_{xx}(B) = \left(\frac{1}{\rho_{xx,1}} + \frac{1}{\rho_{xx,0}} * \frac{1}{\sqrt{1 + (\mu B)^2}} \right)^{-1} \quad (2)$$

The data shown in Fig. 3 agrees well with the magnetoresistive transport predicted by Eq. (2). In the fit to the data $\rho_{xx,1}$, $\rho_{xx,0}$ and μ served as the free parameters, and from the fit we extract the values of $\rho_{xx,1} \sim 30,467 \text{ } \Omega$, $\rho_{xx,0} \sim 5,913 \text{ } \Omega$, and $\mu \sim 0.89 \text{ m}^2/\text{Vs}$. Here, μ is slightly higher than μ_L and is in agreement with values obtained for μ_H near the DP. The B -independent $\rho_{xx,1}$ term is an added correction to the theory, and it has been suggested that the origin of the term is due to $n_e \neq n_h$ and $\mu_e \neq \mu_h$ near the DP.²³

Also included in the $\rho_{xx,1}$ term is the B -independent contribution from grain boundary scattering. Our magnetotransport measurements on a Hall bar that had a longer channel length (L increased by an order of magnitude) displayed a marked decrease in $\Delta\rho_{xx}/\rho_0$ (See Ref. 12). We found $\Delta\rho_{xx}/\rho_0 \sim 80\%$ at $B = 2.6 \text{ T}$ for the Hall bar with $L = 550\mu\text{m}$ compared to $\Delta\rho_{xx}/\rho_0 \sim$

106% at $B = 2.6$ T for the Hall bar with $L = 55\mu\text{m}$, as reported previously (with $W = 5 \mu\text{m}$ for each Hall bar). An increase in L results in an increase in the number of grain boundaries within the film as well as an increase in grain boundary scattering; for example, we found $\rho_s \sim 204 \Omega$ for hole transport with $L = 55 \mu\text{m}$ (as reported previously) and we found $\rho_s \sim 255 \Omega$ for hole transport with $L = 550 \mu\text{m}$, which corresponds to an approximately 25% increase in short range scattering. Therefore, we suggest that a decrease in $\Delta\rho_{xx}/\rho_0$ with increasing L can result from an increase in short-range scattering that can impact the B -independent $\rho_{xx,1}$ value in Eq. (2).

The results of the fit to Eq. (2) allow us to directly compare the magnetotransport observed within our polycrystalline graphene to that observed within an exfoliated graphene crystal. While it is difficult to ascertain the exact contribution from grain boundary scattering to $\rho_{xx,1}$, the ratio $\rho_{xx,0}/\rho_{xx,1}$ can offer a means of comparison between the different forms of graphene (i.e. exfoliated or CVD). For the exfoliated graphene case, it was found that $\rho_{xx,0}/\rho_{xx,1} \sim 0.1$,²³ while we find $\rho_{xx,0}/\rho_{xx,1} \sim 0.19$ for our polycrystalline graphene, which indicates that in each case the B -dependent term in Eq. (2) is still the dominant term. This suggests that the magnetotransport measured in our CVD-derived polycrystalline graphene still produces magnetoresistive transport at the DP comparable to that of exfoliated graphene, despite $L_a \ll L$.

Figure 4(a) shows $\Delta\rho_{xx}/\rho_0$ as a function of B for several values of V_g away from the DP. We found $\Delta\rho_{xx}/\rho_0 \propto V_g^{-1}$ with $\Delta\rho_{xx}/\rho_0$ always being positive. Also shown in Fig. 4(a) is a fit to the data where ρ_{xx} is given by

$$\rho_{xx}(B) = \rho_{xx}(0) \left(1 - \alpha + \left[\frac{\alpha}{\sqrt{1 + 2A(\mu B)^2/\alpha}} \right] \right)^{-1} \quad (3)$$

where α and A are the fitting parameters. For the fits to Eq. (3) we use the measured values of μ_H , which takes into account the small n dependence of μ . Studies have shown that for single-crystal graphene, the dimensionless coefficient A depends upon the average carrier density, n_O , and the density fluctuations, n_{rms} . For the case $n_O \gg n_{rms}$ it was found that $A = (1/2)(n_O/n_{rms})^{-2}$.²⁴ Effective medium theory calculations, taking into account charged impurity disorder, also resulted in a power law dependence of A as a function of the ratio n_O/n_{rms} .²⁴ Figure 4(b) shows the values of A , obtained from the fits shown in Fig. 4(a), versus the ratio n/n_{rms} , where n is measured via the Hall effect (Ref. 12) and n_{rms} is approximated by $n_{rms} \sim \sigma_{min}\sqrt{3}/e\mu$ where σ_{min} is the minimum conductivity measured at $B = 0$ T. The result of the fit shown in Fig. 4(b) is a modified expression for A versus the ratio n_O/n_{rms} , which is given by

$$A = \left[\beta \left(\frac{n_O}{n_{rms}} \right) - \gamma \right]^\eta \quad (4)$$

The values obtained for the constants in Eq. (4) are $\beta = 47$, $\gamma = 94$, and $\eta = -0.29$. That Eq. (4) deviates from the functional form found for the case of single-crystal graphene on SiO₂ (where $\beta = 1/2$, $\gamma = 0$, and $\eta = -2$ is the power of n_O/n_{rms}) is a result of scattering from grain boundaries within our polycrystalline graphene. The result expressed by Eq. (4) is a modified expression for the charge carrier density dependence of the magnetoresistivity with respect to the case of single-crystal graphene. Values for β , γ , and η can be sample dependent, and future studies are needed to determine the relationship between these constants and the measured value of ρ_s (which includes contributions from grain boundary scattering).

IV. Conclusions

Transport in polycrystalline graphene is complex with a delicate interplay between charge and spatial inhomogeneity determining the electronic and magnetotransport. Our results show that, despite $L \gg L_a$, near the DP uncorrelated charge impurity scattering is the dominant scattering mechanism at zero magnetic flux density while scattering from grain boundaries becomes significant as the charge carrier density increases. We find that the magnetotransport is largely dependent upon charge disorder, similar to the case of single-crystal graphene.

Acknowledgments:

The authors gratefully acknowledge the members of the technical staff of the Institute for Nanoscience at NRL, David W. Zapotok and Dean R. St. Amand. This work was supported by the Office of Naval Research. B.R.M. gratefully acknowledges support through the N.R.L. Karles Fellow program.

References:

1. A. Reina, X. Jia, J. Ho, D. Nezich, H. Son, V. Bulovic, M. S. Dresselhaus, and J. Kong, *Nano Lett.* **9** (1), 30-35 (2009).
2. K. S. Kim, Y. Zhao, H. Jang, S. Y. Lee, J. M. Kim, K. S. Kim, J.-H. Ahn, P. Kim, J.-Y. Choi, and B. H. Hong, *Nature* **457**, 706-710 (2009).
3. S. Bae, H. Kim, Y. Lee, X. Xu, J.-S. Park, Y. Zheng, J. Balakrishnan, T. Lei, H. R. Kim, Y. I. Song, Y.-J. Kim, K. S. Kim, B. Özyilmaz, J.-H. Ahn, B. H. Hong, and S. Iijima, *Nature Nanotech.* **5**, 574-578 (2010).
4. X. Li, W. Cai, J. An, S. Kim, J. Nah, D. Yang, R. Piner, A. Velamakanni, I. Jung, E. Tutuc, S. K. Banerjee, L. Colombo, and R. S. Ruoff, *Science* **324**, 1312-1314 (2009).
5. J. C. Koepke, J. D. Wood, D. Estrada, Z.-Y. Ong, K. T. He, E. Pop, and J. W. Lyding, *ACS Nano* **10** (1), 75-86 (2013).

6. Q. Yu, L. A. Jauregui, W. Wu, R. Colby, J. Tian, Z. Su, H. Cao, Z. Liu, D. Pandey, D. Wei, T. F. Chung, P. Peng, N. P. Guisinger, E. A. Stach, J. Bao, S.-S. Pei, and Y. P. Chen, *Nature Mater.* **10**, 443-449 (2011).
7. L. A. Jauregui, H. Cao, W. Wu, Q. Yu, and Y. P. Chen, *Solid State Communications* **151**, 1100-1104 (2011).
8. A. W. Tsen, L. Brown, M. P. Levendorf, F. Ghahari, P. Y. Huang, R. W. Havener, C. S. Ruiz-Vargas, D. A. Muller, P. Kim, and J. Park, *Science* **336**, 1143-1146 (2012).
9. X. C. Yang, H. M. Wang, T. R. Wu, F. Q. Huang, J. Chen, X. X. Kang, Z. Jin, X. M. Xie, and M. H. Jiang, *Appl. Phys. Lett.* **102**, 233503 (2013).
10. H. Cao, Q. Yu, L. A. Jauregui, J. Tian, W. Wu, Z. Liu, R. Jalilian, D. K. Benjamin, Z. Jiang, J. Bao, S. S. Pei, and Y. P. Chen, *Appl. Phys. Lett.* **96**, 122106 (2010).
11. L. G. Cancado, A. Jorio, E. H. Martins Ferreira, F. Stavale, C. A. Achete, R. B. Capaz, M. V. O. Moutinho, A. Lombardo, T. S. Kulmala, and A. C. Ferrari, *Nano Lett.* **11** (8), 3190-3196 (2011).
12. See Supplemental Material at [<http://link.aps.org/supplemental/>] for graphene Hall effect data, related magnetoresistive transport for n_e and n_h , and magnetoresistive data for a Hall bar with $L=550\mu\text{m}$.
13. S. V. Morozov, K. S. Novoselov, M. I. Katsnelson, F. Schedin, D. C. Elias, J. A. Jaszczak, and A. K. Geim, *Phys. Rev. Lett.* **100**, 016602 (2008).
14. J.-H. Chen, W. G. Cullen, C. Jang, M. S. Fuhrer, and E. D. Williams, *Phys. Rev. Lett.* **102**, 236805 (2009).
15. Y.-W. Tan, Y. Zhang, K. Bolotin, Y. Zhao, S. Adam, E. H. Hwang, S. Das Sarma, H. L. Stormer, and P. Kim, *Phys. Rev. Lett.* **99**, 246803 (2007).
16. N. Petrone, C. R. Dean, I. Meric, A. M. van der Zande, P. Y. Huang, L. Wang, D. Muller, K. L. Shepard, and J. Hone, *Nano Lett.* **12**, 2751-2756 (2012).
17. J.-H. Chen, C. Jang, S. Xiao, M. Ishigami, and M. S. Fuhrer, *Nature Nanotech.* **3**, 206-209 (2008).
18. L. Tapasztó, P. Nemes-Incze, G. Dobrik, K. J. Yoo, C. Hwang, and L. P. Biró, *Appl. Phys. Lett.* **100**, 053114 (2012).
19. J. Martin, N. Akerman, G. Ulbricht, T. Lohmann, J. H. Smet, K. Von Klitzing, and A. Yacoby, *Nature Phys.* **4**, 144-148 (2008).
20. R. Jalilian, L. A. Jauregui, G. Lopez, J. Tian, C. Roecker, M. M. Yazdanpanah, R. W. Cohn, I. Jovanovic, and Y. P. Chen, *Nanotechnology* **22**, 295705 (2011).
21. J. Yan, E. A. Henriksen, P. Kim, and A. Pinczuk, *Phys. Rev. Lett.* **101**, 136804 (2008).
22. V. Guttal, and D. Stroud, *Phys. Rev. B* **71**, 201304(R) (2005).
23. S. Cho, and M. S. Fuhrer, *Phys. Rev. B* **77**, 081402(R) (2008).
24. J. Ping, I. Yudhistira, N. Ramakrishnan, S. Cho, S. Adam, and M. S. Fuhrer, *Phys. Rev. Lett.* **113**, 047206 (2014).

Figures:

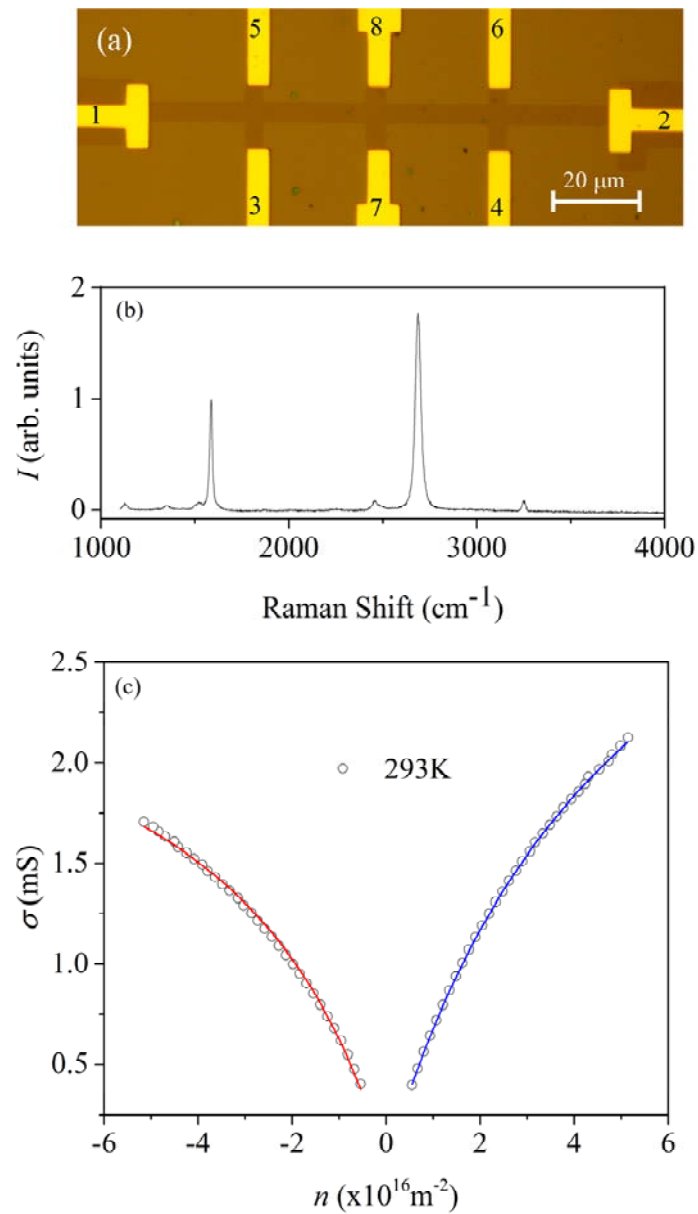


FIG. 1 (color online). (a) Optical image of a graphene Hall bar. Light regions (1-8) are the Cr/Au contacts. The brown background is the SiO₂ substrate. (b) Raman spectrum of polycrystalline graphene, normalized to the G-mode intensity. (c) Conductivity σ versus charge carrier density n at magnetic field $B = 0$ T. The open circles are the experimental data and the solid lines are fits to Eq. (1).

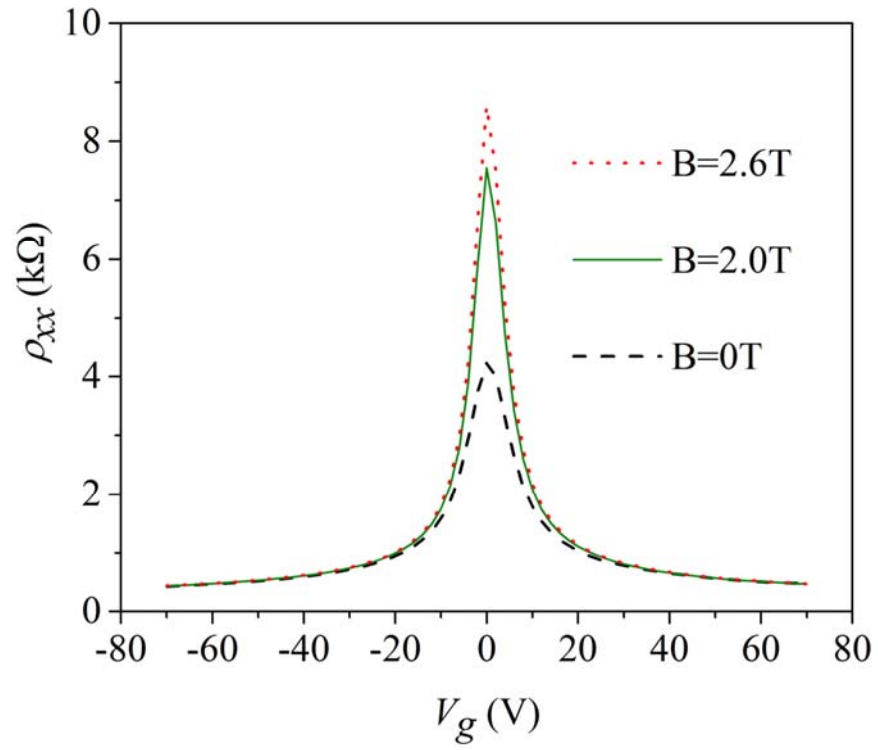


FIG. 2 (color online). Magnetoresistivity ρ_{xx} versus back gate voltage V_g at temperature $T = 293\text{ K}$ for several values of magnetic field B .

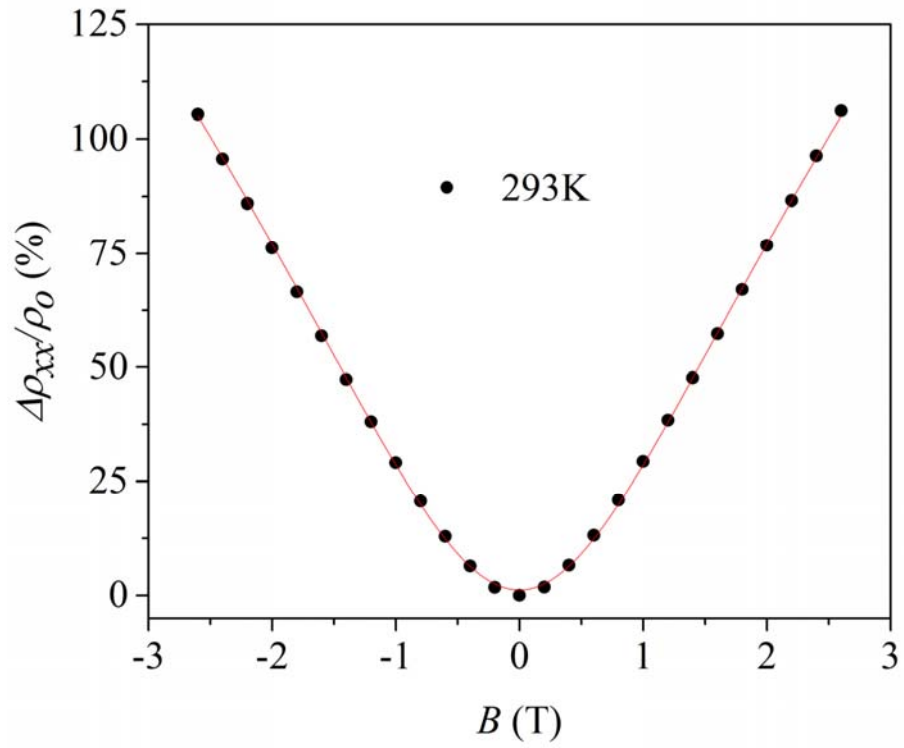


FIG. 3 (color online). Percent change in the magnetoresistivity $\Delta\rho_{xx}/\rho_0$ versus magnetic field B at the DP. The solid line is a fit to Eq. (2).

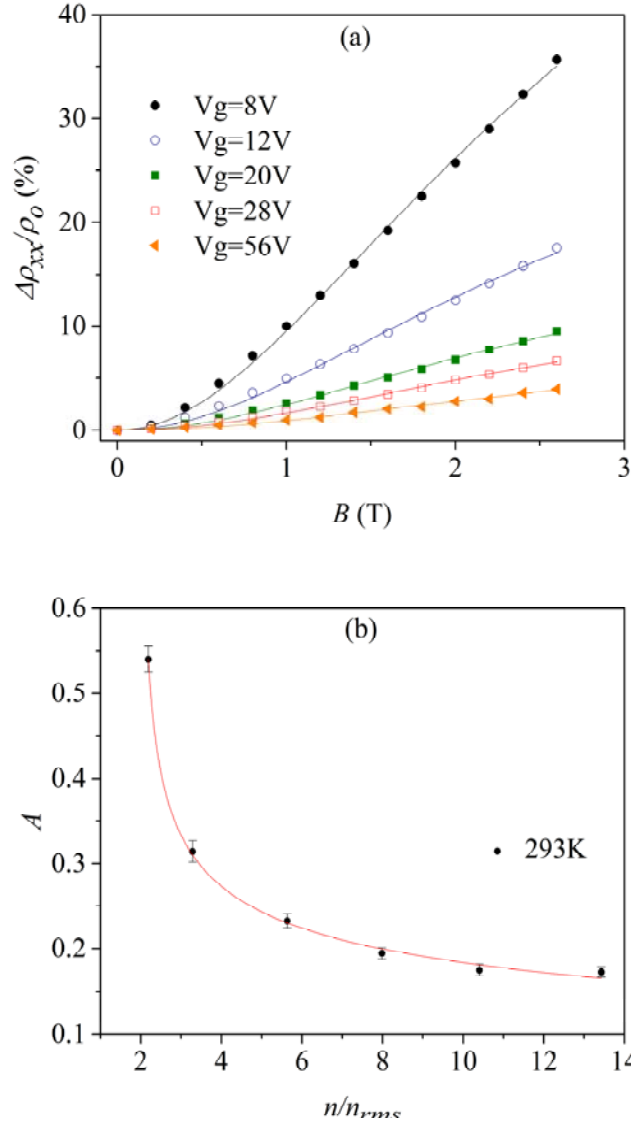


FIG. 4 (color online). (a) Percent change in the magnetoresistivity $\Delta\rho_{xx}/\rho_0$ versus magnetic field B at temperature $T = 293$ K for back gate voltage $V_g = 8$ V ($n_e \sim 5.4 \times 10^{15} \text{ m}^{-2}$), $V_g = 12$ V ($n_e \sim 8.2 \times 10^{15} \text{ m}^{-2}$), $V_g = 20$ V ($n_e \sim 1.4 \times 10^{16} \text{ m}^{-2}$), $V_g = 28$ V ($n_e \sim 2.0 \times 10^{16} \text{ m}^{-2}$), and $V_g = 56$ V ($n_e \sim 4.1 \times 10^{16} \text{ m}^{-2}$). The solid lines are fits to Eq. (3). (b) Dimensionless magnetoresistive coefficient, A , versus the ratio between charge carrier density n and density fluctuations n_{rms} . The solid line is a fit to Eq. (4).